ACS APPLIED MATERIALS & INTERFACES

Research Article

www.acsami.org

Dual-Enzyme Characteristics of Polyvinylpyrrolidone-Capped Iridium Nanoparticles and Their Cellular Protective Effect against H_2O_2-Induced Oxidative Damage

Hua Su,[†] Dan-Dan Liu,[‡] Meng Zhao,[†] Wei-Liang Hu,[†] Shan-Shan Xue,[†] Qian Cao,[†] Xue-Yi Le,[‡] Liang-Nian Ji,[†] and Zong-Wan Mao*[,†,‡]

[†]MOE Key Laboratory of Bioinorganic and Synthetic Chemistry, School of Chemistry and Chemical Engineering, Sun Yat-Sen University, Guangzhou 510275, P. R. China

[‡]Department of Applied Chemistry, South China Agricultural University, Guangzhou 510642, P. R. China

Supporting Information

ABSTRACT: Polyvinylpyrrolidone-stabilized iridium nanoparticles (PVP-IrNPs), synthesized by the facile alcoholic reduction method using abundantly available PVP as protecting agents, were first reported as enzyme mimics showing intrinsic catalase- and peroxidase-like activities. The preparation procedure was much easier and more importantly, kinetic studies found that the catalytic activity of PVP-IrNPs was comparable to previously reported platinum nanoparticles. Transmission electron microscopy (TEM) and X-ray photoelectron spectroscopy (XPS) characterization indicated that PVP-IrNPs had the average size of approximately 1.5 nm and mainly consisted of Ir(0) chemical state. The mechanism of PVP-IrNPs' dual-enzyme activities was investigated using XPS, Electron spin resonance (ESR) and cytochrome C-based electron transfer methods. The catalase-like activity was related to the formation of oxidized species Ir(0)@IrO_2 upon reaction with H_2O_2. The peroxidase-like activity originated from their ability acting as electron transfer mediators during the catalysis cycle, without the production of hydroxyl radicals. Interestingly, the protective effect of PVP-IrNPs against H_2O_2-induced cellular oxidative damage was investigated in an A549 lung cancer cell model and PVP-IrNPs displayed excellent biocompatibility and antioxidant activity. Upon pretreatment of cells with PVP-IrNPs, the intracellular reactive oxygen species (ROS) level in response to H_2O_2 was decreased and the cell viability increased. This work will facilitate studies on the mechanism and biomedical application of nanomaterials-based enzyme mimic.

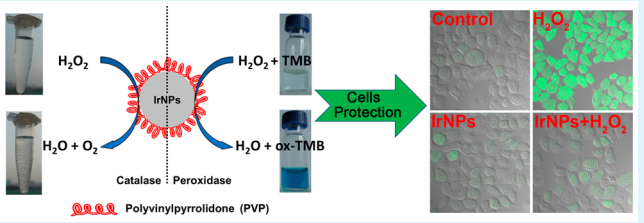

KEYWORDS: *iridium nanoparticles, polyvinylpyrrolidone, catalase- and peroxidase-like activity, catalytic mechanism, H_2O_2-induced cytotoxicity reduction, antioxidants*

1. INTRODUCTION

As an important transition-metal element, iridium has attracted much interest these years for application in catalysis,[1−5] fluorescent labeling,[6,7] molecular sensing,[8,9] OLED,[10] and biocompatible coatings of coronary stents.[11] In the field of catalysis, iridium-based catalyst has been recognized as an outstanding candidate because of its high activity, stability and stereoselectivity.[12−14] Among all the noble metal-based electrocatalysts, only iridium has been found displaying high activities for both oxygen reduction reaction (ORR) and oxygen evolution reaction (OER) under acidic condition.[15] In particular, iridium-based nanomaterials have shown different physical and chemical properties from the bulk counterparts based on their high surface-to-volume ratio and high density of active sites.[16,17] This promotes the exploration of the new properties and potentials of iridium-based nanomaterials.

Recent development in inorganic nanomaterials promoted the arising of nanoscaled enzyme mimics,[18,19] so-called nanozymes, mainly due to their higher stability and intrinsic catalytic activity comparable to natural enzymes. Since the first report on Fe_3O_4 nanoparticles possessing intrinsic peroxidase-like activity in 2007,[20] an increasing number of nanomaterials such as metal oxide,[21,22] transition metal chalcogenide,[15,23] carbon nanostructures,[24,25] metal nanoparticles[26−29] and others[30,31] has been exploited as enzyme mimics. Among them, noble metal-based nanozymes have received tremendous interests which displayed substantial advantages in easier preparation procedures, size/surface facet-tunable catalytic activities and high stability. To date, gold,[32] silver,[33] platinum,[34] palladium,[35] ruthenium,[22] silver/platinum,[36] and palladium/gold[37]-based nanozymes have been investigated and used for antibiotics detection,[32] glucose sensing,[33] oxygen-stress reduction,[34] glucose oxidation,[35] cancer cell detection[37] and so on. In particular, Pt-based nanozymes were quite fascinating candidates due to their small size, excellent catalytic activity and good biocompatibility.[28,34,38,39] Unfortunately, the preparation

Received: February 9, 2015
Accepted: March 31, 2015
Published: March 31, 2015

DOI: 10.1021/acsami.5b01271
ACS Appl. Mater. Interfaces 2015, 7, 8233−8242

process of these small-sized Pt-based nanozymes was usually tedious and time-consuming, because expensive template molecules (ferritin, lysozyme or polyamidoamine dendrimer), strict control of reaction conditions and complex purification procedures were generally necessary. Early study has reported that the size of iridium nanoparticles was smaller than platinum nanoparticles under the same synthetic conditions, which was attributed to slower nucleation and growth of iridium.[40] This prompted us to consider the feasibility of iridium nanomaterials acting as nanozymes. Moreover, to the best of our knowledge, iridium-based nanozyme has not been reported yet, although early study have found that Ir metal powder without any surface stabilization agents could decompose H_2O_2 as Pt metal powder did.[41]

In addition to high catalytic activity, good water dispersibility and excellent biocompatibility are also important factors of an ideal enzyme mimic for practical application.[18,19] Polyvinylpyrrolidone (PVP) is a low cost, commercial available, biodegradable and water-soluble polymer[42] and has been frequently used in stabilizing noble metal nanomaterials.[35,43] Moreover, PVP can weakly stabilize metal nanoparticles through multiple coordination of the N−C═O sites,[44] which is very important for substrates accessory during enzyme catalysis. Third, neutral polymer PVP can bind organic molecule at the hydrophobic sites on the random-coiled chain,[45] maybe beneficial for catalysis. Inspired by this, PVP-stabilized iridium nanoparticles (PVP-IrNPs) were prepared in the present work in one-pot reaction by using a green alcoholic reduction method, in which toxic reducing agent $NaBH_4$ was avoided. The results demonstrated that PVP-IrNPs had both intrinsic catalase- and peroxidase-like activities. The steady-state kinetics assay and catalytic mechanism of PVP-IrNPs were investigated in details. Moreover, the biocompatibility of PVP-IrNPs and their potential acting as antioxidant enzyme mimic was also verified in an A549 lung cancer cell model.

2. EXPERIMENTAL SECTION

2.1. Chemicals and Reagents. $IrCl_3 \cdot 3H_2O$ (99.9%, metal basis), 3-carbamoyl-2,2,5,5-tetramethyl-3-pyrrolin-1-yloxy (CTPO, 99%) and Rhodamine B was obtained from Alfa Aesar. Catalase from bovine liver (2000−5000 U mg^{-1}), peroxidase from horseradish VI (250−330 U mg^{-1}), cytochrome C from horse heart (≥99.0%), 2′,7′-dichlorofluorescein diacetate (DCFH-DA), 3-(4,5-dimethylthiazol-2-yl)-2,5-diphenyltetrazolium Bromide (MTT), KH_2PO_4(≥99.0%), Na_2HPO_4(≥99.0%) and KCl (≥99.0%) were purchased from Sigma-Aldrich. 3,3′,5,5′-tetramethylbenzidine (TMB), polyvinylpyrrolidone (PVP, average MW58000, K29−32), iridium standard solution (1000 μg mL^{-1} Ir in 2.0 M HCl solution) and spin traps 5,5-dimethyl-1-pyrroline N-oxide (DMPO, 97%) were purchased from Aladdin Industrial Corporation. Hydrogen peroxide (30%), anhydrous ethanol, hydrochloric acid (36%), nitric acid, sulfuric acid (98%) were purchased from Guangzhou Chemical Reagent Factory and used as received. Catalase assay kit was obtained from Beyotime Institute of Biotechnology. Millipore water (18.2 MΩ) was used throughout the experiments.

2.2. Synthesis of PVP-IrNPs. PVP-stabilized colloidal iridium nanoparticles were synthesized from the alcoholic reduction of precursor $IrCl_3$ solution in the presence of PVP, according to former procedures with some modifications.[17,40] In a typical synthesis, an aqueous solution of $IrCl_3$ (8.4 μmol, 4 mL) was added dropwise into a vigorously stirring 4 mL of ethanol solution containing PVP (18.6 mg, 168 μmol as monomeric unit). Followed by stirring for 12 h at room temperature, a clear pale yellow solution was obtained and then refluxed at 100 °C in air for 6 h. The resulting brown solution was evaporated to completely remove the solvents and the black solid was redissolved in water. The concentration was adjust to 2.5 mg mL^{-1} containing 0.189 mg mL^{-1} iridium according to ICP-MS results and stored at room temperature for direct use.

2.3. Characterization. TEM images and TEM-based energy-dispersive X-ray (EDX) measurements were taken on a JEOL JEM-2010HR transmission electron microscope, with accelerating voltage of 200 kV. Samples for TEM measurements were deposited on a carbon film supported by 300-mesh copper grids. The surface analysis was performed by X-ray photoelectron spectroscopy (XPS) using a Thermo-VG Scientific ESCALAB 250 spectrometer. Photoelectrons were generated by mono Al Kα X-ray radiation of energy 1486.6 eV and the calibration was based on the C 1s with the binding energy at 284.8 eV. Samples for XPS analysis were prepared by depositing aqueous solutions of PVP-IrNPs or $IrCl_3$-PVP onto a piranha solution- and aqua regia-treated silicon wafer and drying in air at room temperature for 1 day. All spectral peaks were deconvoluted by the XPSPEAK version 4.1 software with a Shirley background subtraction and fitted by Gaussian−Lorentzian functions. The concentration of iridium was measured using a Thermo inductively coupled plasma mass spectrometry (ICP-MS) XSERIES 2. Samples for ICP-MS analysis were prepared by dissolving PVP-IrNPs in boiling aqua regia for 3 h, diluting with ultrapure water and filtering with 0.22 μm membrane (Jinteng, China). Catalase kinetics assay and cell viability test were performed on Tecan infinite M200 pro spectrophotometer (Switzerland). Absorption spectra and peroxidase kinetics assay were carried out on a Varian Cary 300 UV−vis spectrometer. ROS determination was performed on confocal laser microscopy (LSM 710, Carl Zeiss, Göttingen, Germany).

2.4. Electron Spin Resonance Experiment. All ESR measurements were carried out using a Bruker EMX A300 spectrometer at ambient temperature. Sample solutions (50 μL) were put in glass capillary tubes with internal diameters of 1 mm and sealed. The tubes were inserted into the ESR cavity and measured at selected times.

ESR parameter settings were as follows: modulation amplitude 1 G, scan range 100 G, microwave power 20 mW and time constant 163.84 ms for detection of spin adducts using spin traps DMPO and modulation amplitude 0.04 G, scan range 5 G, and microwave power 1 mW and time constant 5242.88 ms for ESR oximetry using CTPO.

The catalase activity of PVP-IrNPs was first evaluated in the H_2O_2/UV system. It is well-known that H_2O_2 produces hydroxyl radical under UV irradiation. Spin trap DMPO was used to trap the $^{\bullet}OH$ to form the stable DMPO/$^{\bullet}OH$ spin adduct, which yields the typical four lines ESR spectrum with relative intensities 1:2:2:1.The effect of PVP-IrNPs on the system was studied and compared to that of catalase. Tubes containing 50 mM DMPO, 5 mM H_2O_2 and various concentrations of PVP-IrNPs or catalase in phosphate buffer (pH = 7.0) were exposed to UV light (355 nm) for 10 min and immediately characterized. ESR spin label oximetry is a quantitative approach to measure oxygen content using the water-soluble spin label CTPO. 0.1 mM CTPO solution was mixed with different concentrations of H_2O_2 in phosphate buffer and bubbled with nitrogen for 15 min. Followed by addition of 125 μg mL^{-1} PVP-IrNPs or 2 U mL^{-1} catalase and incubation for 5 min, the ESR spectrum was immediately recorded.

ESR was also used to investigate the interaction mechanism of PVP-IrNPs with H_2O_2 using spin trap DMPO, which can trap short-lived $^{\bullet}OH$. The hydrogen peroxide solution (5 mM) was mixed with DMPO (50 mM) in HCl-KCl buffers (pH = 1.2) and the reaction was initiated by addition of various concentrations of PVP-IrNPs (3.125−62.5 μg mL^{-1}). After 5 min incubation in the dark at room temperature, the ESR spectrum was immediately recorded.

2.5. Catalase-like Activity Assay. The catalase-like activity assays were carried out at 37 °C using catalase assay kit according to the manufacturer's instructions. Ten μL of PVP-IrNPs solution (625 μg mL^{-1}, containing 47.25 μg mL^{-1} Ir) or catalase solution (10 μg mL^{-1}) were added to 50 μL Teorell-Stenhagen buffer (T-S buffer, 33 mM citric acid, 33 mM phosphoric acid, 23 mM boric acid, pH = 7.0) in the presence of varied concentrations of H_2O_2. After 5 min reaction, the solution was diluted 50 times by T-S buffer and then the residual H_2O_2 was monitored at 520 nm using Tecan infinite 200 pro spectrophotometer. In order to study the effects of pH and temperature on the activities of PVP-IrNPs and catalase, the

DOI: 10.1021/acsami.5b01271
ACS Appl. Mater. Interfaces 2015, 7, 8233−8242

concentration of H_2O_2 was fixed at 50 mM, while pH and temperature range are 3−12 and 4−75 °C, respectively. The apparent kinetic parameters were calculated using the Lineweaver−Burk plot, $1/V = 1/V_{max}+K_M/(V_{max}\ C)$, where V is the initial velocity, V_{max} is the maximal reaction velocity, C is the concentration of the substrate and K_M is the Michaelis−Menten constant.

2.6. Peroxidase-like Activity Assay. The kinetic assays were carried out at room temperature in 500 μL of phosphate buffer with 625 ng mL^{-1} PVP-IrNPs (47.25 ng mL^{-1} Ir) or 1 ng mL^{-1} peroxidase in the presence of H_2O_2 and TMB. The steady-state kinetic analysis of PVP-IrNPs with H_2O_2 as the substrate was performed by varying the concentrations of TMB at fixed H_2O_2 concentration and vice versa in phosphate buffer (25 mM, pH 4.5) at room temperature. To study the effects of pH and temperature on the activities of PVP-IrNPs compared to that of peroxidase, the reaction were carried out pH 2−10 and 25−75 °C, in the presence of 50 mM H_2O_2 and 500 μM TMB. All the reactions were monitored in timescan mode at 652 nm belonging to oxidized TMB product using a Cary 300 UV−vis spectrophotometer and all operations were done at room temperature and in the dark. The apparent kinetic parameters were calculated based on the Michaelis equation $V=V_{max}\ C/(K_M+C)$, where V is the initial velocity, V_{max} is the maximal reaction velocity, C is the concentration of the substrate, and K_M is the Michaelis−Menten constant.

2.7. Rhodamine B Oxidation Experiment. Degradation of Rhodamine B is often used to verify peroxidase-like abilities to catalyze H_2O_2 to oxidize organic molecule through production of hydroxyl radicals.[46] In our experiment, 15 μL of H_2O_2 aqueous solution (5 mM) was added into a mixture solution of Rhodamine B (50 μM) and PVP-IrNPs (varied concentrations) to initiate the reaction. Followed by 3.5 h incubation in the dark at room temperature, the resulting solution was diluted 2-fold for UV−vis absorbance characterization. The peak absorbance of Rhodamine B lies at 550 nm.

2.8. Cytochrome C Electron Transfer Experiment. Cytochrome C (Cyt C) is an active reactant in electron transfer process and has been used to understand electron transfer mediator role of Co_3O_4 nanoparticles.[47] In our experiment, varied amounts of PVP-IrNPs were added into a phosphate buffer solution (25 mM, pH = 4.5) containing 400 μM Cyt C. Followed by 1 h incubation in the dark at room temperature, the resulting solution was characterized by UV−vis absorbance spectrometer. In order to know whether Cyt C was oxidized by dissolved oxygen, we pumped the stock solutions of Cyt C, PVP-IrNPs solution and buffer simultaneously with pure N_2 for 0.5 h and repeated above experiments.

2.9. Cell Culture and Viability Assay. A549 human lung cancer cells were obtained from Experimental Animal Center of Sun Yat-Sen University (Guangzhou, China). Cells were cultured in RPMI 1640 (Roswell Park Memorial Institute 1640, Gibco BRL) medium containing 10% FBS (fetal bovine serum, Gibco BRL), 100 μg mL^{-1} streptomycin and 100 U mL^{-1} penicillin (Gibco BRL). The cells were seeded in 96-well plate at 8000 cells per well in a humidified incubator at 37 °C with an atmosphere of 5% CO_2 and 95% air. After overnight incubation, the cells were treated with varied concentrations of PVP-IrNPs diluted with RPMI 1640 medium containing 10% FBS. After incubation for 20 h, 20 μL MTT in PBS (5 mg mL^{-1}) was added to each well. The cells were incubated for another 4 h. At the end of the incubation time, the medium was removed and the formed formazan was dissolved in DMSO (150 μL). The cell viability was evaluated by measurement of the absorbance at 595 nm (Infinite F200, Tecan, Switzerland). The protective effect of PVP-IrNPs on A549 cells against H_2O_2-induced oxidative damage was also checked by MTT assay. After incubation of A549 cells with varied concentrations of PVP-IrNPs for 24 h, the medium was carefully removed and washed once with PBS. Upon addition of 1 mM H_2O_2 into each wells, the cells were incubated another 1h in an incubator at 37 °C and 5% CO_2. Followed by washing with PBS once again, the cells were added new RPMI 1640 medium containing MTT before further viability assay.

2.10. Determination of Intracellular ROS. The intracellular ROS was determined by the DCFH-DA assay.[34] Briefly, A549 cells were seeded into 35 mm dishes at a density of about 1.5×10^5 cells per well and incubated overnight at 37 °C and 5% CO_2. Upon treatment without or with 250 μg mL^{-1} PVP-IrNPs for 20 h, the cells were carefully rinsed twice with PBS and incubated with 50 μM DCFH-DA in FBS-free RPMI 1640 medium for 15 min in the dark. The cells were further rinsed twice with PBS and then exposed to 1 mM H_2O_2 in PBS for 45 min at 37 °C. The cells were carefully rinsed again and the intracellular ROS levels were determined with confocal laser microscopy with excitation wavelength at 488 nm.

3. RESULTS AND DISCUSSION

3.1. Synthesis and Characterization of PVP-IrNPs. PVP-IrNPs were prepared using a modified alcoholic reduction strategy based on the previous report by Kobayashi[17] and Hirai[40] et al. The synthetic procedure is simple and green, as it avoids the utilization of $NaBH_4$ which is harmful to organisms and environment (Figure 1A). The generation of colloidal

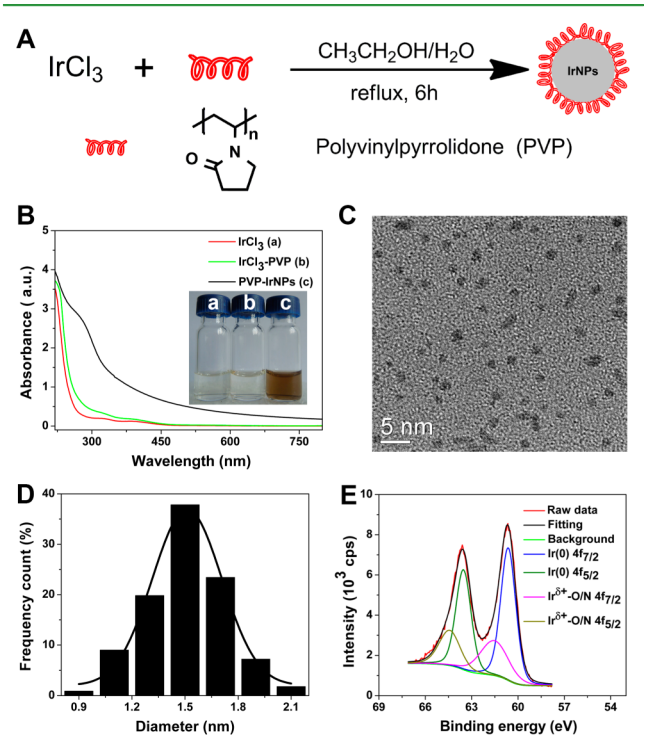

Figure 1. Presented are (A) Synthetic scheme (B) UV−vis absorbance, (C) TEM images, (D) size distribution analysis from 200 random nanoparticles and (E) High resolution XPS Ir 4f scan of PVP-IrNPs. Insets in (B) were optical images of aqueous solutions of $IrCl_3$, mixture of $IrCl_3$ and PVP without heating ($IrCl_3$-PVP) and PVP-IrNPs.

IrNPs was visualized during the reflux (see inset of Figure 1B), where the color of the reaction mixture changed from pale yellow to light brown, indicating the transitions from the initially formed $IrCl_3$-PVP to the final product PVP-IrNPs. UV−vis spectrum of $IrCl_3$-PVP showed two absorption hump peaks at about 330 and 400 nm, similar to $IrCl_3$ solution. Following thermolytic reduction, these absorption peaks disappeared and a new peak appeared at 280 nm (Figure 1B), further indicating the formation of PVP-IrNPs.[14] Transmission electron microscopy (TEM) analysis clearly showed that the as-synthesized PVP-IrNPs were of quasi-spherical shape and apparent agglomeration was not observed (Figure 1C). This could be rationalized as the stabilizing effect of PVP based on the steric hindrance. Energy dispersive X-ray (EDX) spectrum verified the presence of iridium in the PVP-stabilized nanoparticles (Supporting Information Figure S1). To obtain a

DOI: 10.1021/acsami.5b01271
ACS Appl. Mater. Interfaces 2015, 7, 8233−8242

reliable size distribution, we carried out a statistical analysis of 200 nanoparticles according to TEM results and found that the diameters of PVP-IrNPs mainly distributed in the 1−2 nm region with the average size of approximately 1.5 nm (Figure 1D), similar to previously reported PVP-protected Ir nanoparticles.[17]

X-ray photon electron spectroscopy (XPS) was used to identify chemical state and surface properties of as-synthesized PVP-IrNPs. High resolution spectra in the Ir 4f regions revealed two chemical state: Ir(0) characterized by $4f_{7/2}$ and $4f_{5/2}$ with binding energies of 60.63 and 63.53 eV,[48] respectively; and $Ir^{\delta+}$−O/N of 61.53 and 64.53 eV (Figure 1E).[49] Quantitative analysis of XPS indicated that the ratio of Ir(0): $Ir^{\delta+}$−O/N was close to 2:1. The binding energy of all iridium peaks for PVP-IrNPs was lower than 62.0 eV, ruling out the nature of IrO_2.[50] High resolution spectra of O 1s regions showed O═C−N (PVP) and $Ir^{\delta+}$−O (OH/O═C−N) at 531.21 and 532.33 eV, respectively (Supporting Information Figure S2C). A new peak at 400.6 eV with lower electron density than that of free PVP,[51] indicated the coordination of nitrogen atom of pyrrole group of PVP to iridium atoms in the case of PVP-IrNPs (Supporting Information Figure S2D). In contrast, $IrCl_3$-PVP mixture showed quite different chemical state (Supporting Information Figure S3). To sum up, PVP-IrNPs were composed of Ir (0) and $Ir^{\delta+}$−O/N state (not IrO_2) and more importantly, pyrrole groups of PVP coordinated to iridium nanoparticles through O and N atoms.

3.2. Catalase-like Activity of PVP-IrNPs. To evaluate the catalase-like activity of water-stable PVP-IrNPs, two approaches with respect to the reactant H_2O_2 and the product O_2 were conducted. The first method is a UV/H_2O_2 system (ESR), employing DMPO as the spin trap to investigate the interaction of PVP-IrNPs with H_2O_2. It is known that •OH radical was produced when H_2O_2 was irradiated with UV light, and the resultant spin adduct DMPO/•OH was ESR active. The H_2O_2 decomposition by catalase would reduce the UV-induced •OH radical production from H_2O_2.Therefore, the ESR signals of spin adduct reflected the interactions of catalase with H_2O_2. As shown in Figure 2 A and B, both natural catalase and PVP-IrNPs reduced the •OH signal in a concentration-dependent manner.

The second method is ESR spin oximetry monitoring the O_2 production in the H_2O_2 degradation reaction. The principle is based on the bimolecular collision of oxygen molecule with a spin probe (CTPO often used), so-called Heisenberg spin exchange process,[52] in which the ESR hyperfine structure of CTPO correlated with O_2 concentration. As shown in Figure 2C and D, the gradual diminution of hyperfine peak was observed in both cases, indicating the enhanced production of O_2 in the H_2O_2 degradation reaction catalyzed by PVP-IrNPs and catalase. Figure 2C and D showed that the PVP-IrNPs displayed catalytic activity in a H_2O_2 concentration-dependent manner, similar to the case of catalase. Simultaneously, O_2 bubbles were clearly observed by naked eyes (Figure 2E). We also checked the interaction of Ir^{3+} or $IrCl_3$-PVP with H_2O_2 and no bubbles were observed (data not shown). All these results provided direct evidence supporting that PVP-IrNPs acted as a functional mimic of catalase.

We also investigated the effect of pH and temperature on the catalytic activity of PVP-IrNPs. Figure 3A and B showed that the optimum condition for natural catalase was pH 8 and 37 °C. It can be explained that structure of natural catalase is quite sensitive to pH and temperature and denatured enzyme

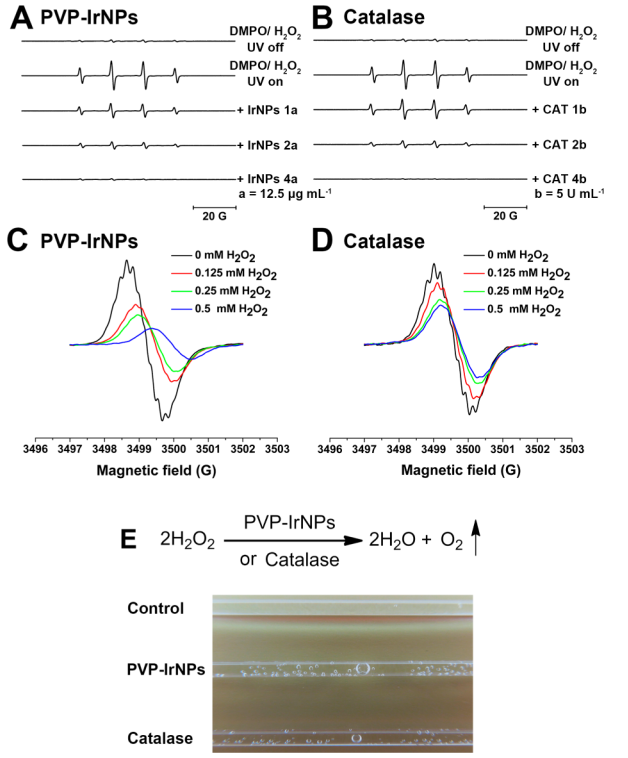

Figure 2. Effect of PVP-IrNPs (A) and catalase (B) on the hydroxyl radical production in a concentration-dependent manner in H_2O_2/UV system. H_2O_2 concentration-dependent oxygen production (ESR spin label oximetry) catalyzed by PVP-IrNPs and catalase were shown (C) and (D), respectively. Gas bubbles were observed after incubation of H_2O_2 and PVP-IrNPs/catalase in phosphate buffer (pH = 7) for 30 min (E): Control, 5 mM H_2O_2; PVP-IrNPs, 125 μg mL^{-1} PVP-IrNPs +5 mM H_2O_2; Catalase, 1 μg mL^{-1} catalase + 5 mM H_2O_2.

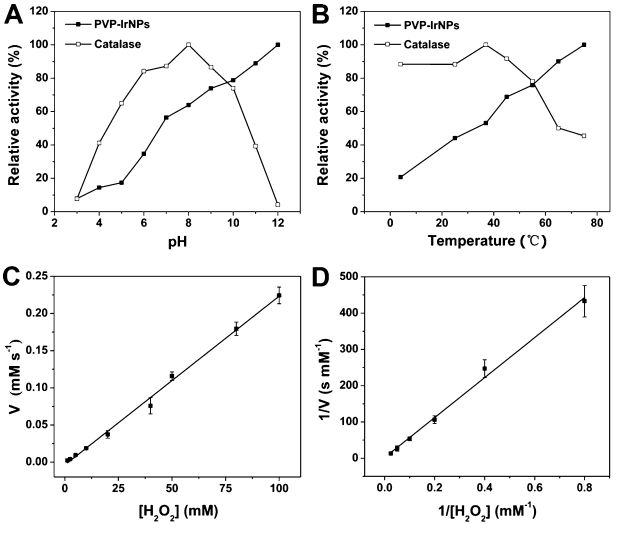

Figure 3. Effect of pH (A) and temperature (B) on the catalase activity of PVP-IrNPs and natural enzyme. (C) Steady state kinetic assay of catalase-like activity of PVP-IrNPs in Teorell-Stenhagen buffer (pH = 7.0) at room temperature. (D) Double-reciprocal plots of activity of PVP-IrNPs at fixed concentration of enzyme versus varying concentration of H_2O_2.

inevitably leads to decreased activity. In contrast, catalase-like activity of PVP-IrNPs continued to increase with rising pH and temperature up to pH 12 and 75 °C (Figure 3A and B),

DOI: 10.1021/acsami.5b01271
ACS Appl. Mater. Interfaces 2015, 7, 8233−8242

Table 1. Kinetic Parameters of Catalase- and Peroxidase-like Activities of PVP-IrNPs and Other Reported Typical Enzyme Mimic

enzyme	$[E]$ (M)[a]	substrate	K_M (mM)	V_{max} (10^{-3} mM s^{-1})	k_{cat}[b] (10^3 s^{-1})	k_{cat}/area[c] (s^{-1} nm^{-2})	ref
				catalase activity			
PVP-IrNPs	~3.94 × 10^{-7}	H_2O_2	297	540	1.37	194	this work
Ft-PtNPs	~1.89 × 10^{-7}	H_2O_2	421	840	4.46	406	28
Ac-G9/PtNPs	1 × 10^{-8}	H_2O_2	126	82.5	8.25	241	38
				peroxidase activity			
PVP-IrNPs	~1.97 × 10^{-9}	H_2O_2	266	0.385	0.196	27.7	this work
		TMB	0.02	0.108	0.055	7.76	
Ft-PtNPs	~4.24 × 10^{-8}	H_2O_2	187	320	7.55	687	28
		TMB	0.22	0.558	0.0132	1.2	
Co_3O_4	2.53 × 10^{-9}	H_2O_2	174	0.189	0.0747	0.459	47
		TMB	0.103	0.256	0.101	0.622	
Fe_3O_4	1.14 × 10^{-12}	H_2O_2	154	0.0978	85.8	0.303	20
		TMB	0.098	0.0344	30.2	0.107	

[a] $[E]$ is the concentration of nanoparticles and estimated from the nanoparticle size and the amount of metal element according to the equation $[E] = (m/(4/3\ \pi\ (D/2)^3\ \rho_M))/N_A$,[20] m is mass concentration of nanoparticles, D is average diameter of nanoparticles, ρ_M is the density of corresponding metal, and N_A is the Avogadro constant. [b] k_{cat} is the catalytic constant per nanoparticle, where $k_{cat} = V_{max}/[E]$. [c] area is surface area per nanoparticle, which is estimated from D according to equation area = $\pi\ D^2$.

respectively. It should be noted that the effect of pH and temperature on the self-decomposition of H_2O_2 has been offset. The enhanced activity of PVP-IrNPs at higher pH value, may be attributed to higher stability of PVP-IrNPs than natural catalase, and lower redox potential of H_2O_2/O_2 at higher pH[47] (much easier catalytic decomposition of H_2O_2 by iridium nanoparticles in neutral and basic conditions). The increased activity of PVP-IrNPs with elevated temperature can also be explained by high stability of PVP-IrNPs and the Arrhenius equation.[28] Therefore, PVP-IrNPs are promising catalase mimic particularly in high pH and high temperature conditions.

To calculate the enzymatic parameters, we studied the steady-state kinetics of PVP-IrNPs by measuring the initial rates as a function of H_2O_2 concentration. The catalytic process follows the typical Michiaelis-Menten reaction and the corresponding Lineweaver−Burk plots can be obtained (Figure 3C and D). As shown in Table 1, The apparent K_M value of PVP-IrNPs with H_2O_2 was 297 mM, comparable with that of the reported platinum nanoparticles (421 mM for Ft-PtNPs[28] and 126 mM for Ac-G9/PtNPs[38]) but nearly three times higher than catalase (71.6 mM),[28] suggesting a relatively lower affinity of PVP-IrNPs to H_2O_2 in comparison to catalase. The relatively smaller k_{cat} value of PVP-IrNPs (1370 s^{-1}) indicated slightly lower catalytic activity than platinum nanoparticles, which possessed relatively bigger k_{cat} values (4460 s^{-1} for Ft-PtNPs[28] and 8250 s^{-1} for Ac-G9/PtNPs[38]). It should be noted that the enzyme-like activity of nanoparticles mainly originated from the catalytically active sites on the nanomaterial surface, therefore it is expected that nanoparticle with larger size could expose more active centers.[47] To eliminate the difference in activity caused by various sizes, the catalytic efficiency was normalized by particle surface area. It was found that the normalized catalytic efficiency of PVP-IrNPs was comparable to the reported platinum nanoparticles (194 s^{-1} nm^{-2} for PVP-IrNPs, 406 s^{-1} nm^{-2} for Ft-PtNPs, and 241 s^{-1} nm^{-2} for Ac-G9/PtNPs), indicating the potential of iridium nanoparticles acting as catalase mimic.

XPS technique was used to investigate the reaction mechanism of PVP-IrNPs with H_2O_2. Low concentration of H_2O_2 (50 mM) displayed negligible effect on the binding energy of PVP-IrNPs (Supporting Information Figure S6A). However, upon high concentration of H_2O_2 treatment (Figure 4), the binding energy of Ir 4f shifted to higher level suggesting

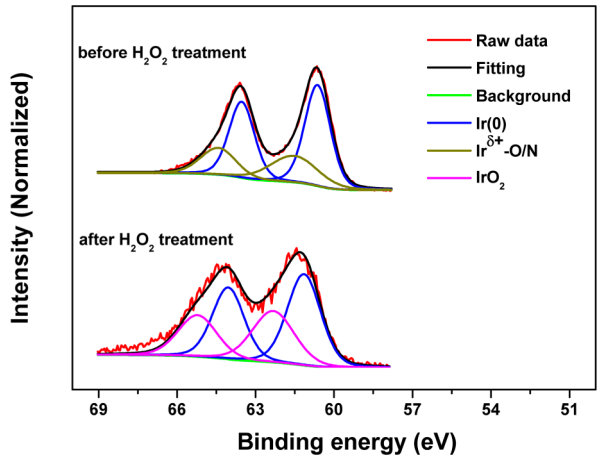

Figure 4. Ir 4f XPS spectra of PVP-IrNPs before and after 5 M H_2O_2 treatment.

decreased electronic density of iridium element. Spectra fitting with Gaussian−Lorentzian functions revealed that IrO_2 species formed on the surface of Ir(0) core upon H_2O_2 treatment.[53] The Ir 4f level of Ir(0) core also shifted to slightly higher level, which might be attributed to the presence of IrO_2 species on the surface.[49] The equation can be written as follows:

$$Ir(0)@Ir^{\delta+}—O/N + H_2O_2 \rightarrow Ir(0)@IrO_2 + H_2O$$

Combined with early assumption from the electrochemical results that an incomplete monomolecular layer formed on the surface of iridium electrode upon reaction with H_2O_2,[54] we assumed that the formed oxidized species $Ir(0)@IrO_2$ then catalyzed other H_2O_2 molecules to produce oxygen and water.

3.3. Peroxidase-like Activity of PVP-IrNPs. To explore the activity of PVP-IrNPs acting as peroxidase mimic, the catalysis of peroxidase substrate TMB was tested in the presence of H_2O_2, as shown in Figure 5A and B. It can be seen that PVP-IrNPs can catalyze the oxidation of TMB by H_2O_2 to produce typical blue product, which had maximum absorbance

DOI: 10.1021/acsami.5b01271
ACS Appl. Mater. Interfaces 2015, 7, 8233−8242

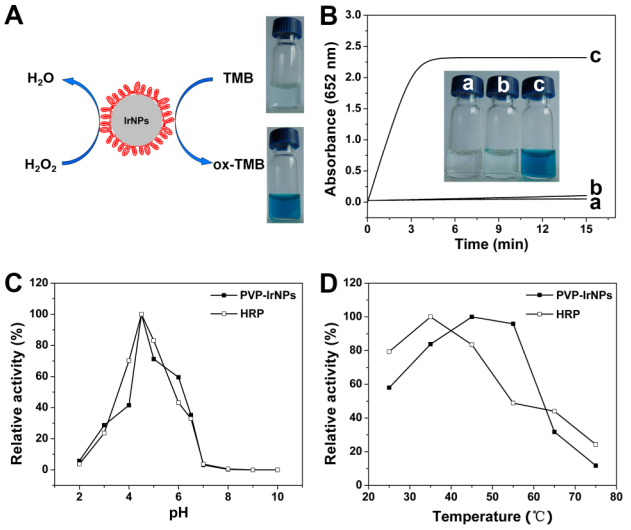

Figure 5. (A) Schematic illustration of peroxidase activities of PVP-IrNPs. (B)Time-dependent absorption at 652 nm in different reaction systems: (a) PVP-IrNPs + TMB, (b) TMB + H_2O_2, and (c) PVP-IrNPs + TMB + H_2O_2. The effect of pH (C) and temperature (D) on the peroxidase activity of PVP-IrNPs and HRP.

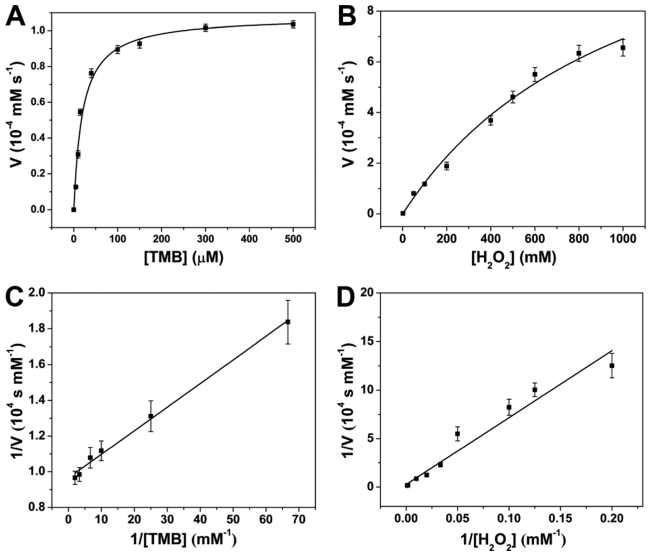

Figure 6. Steady state kinetic assay of peroxidase-like activity of PVP-IrNPs in phosphate buffer (25 mM, pH 4.5) at room temperature. (A) The H_2O_2 concentration was 50 mM and TMB was varied. (B)TMB concentration was fixed at 500 μM and H_2O_2 was varied. (C, D) were double-reciprocal plots of activity of PVP-IrNPs, corresponding to (A, B).

at 652 nm, indicating the peroxidase-like activity of PVP-IrNPs (Supporting Information Scheme S1). In contrast, TMB showed negligible color change in the absence of PVP-IrNPs or H_2O_2. Neither $IrCl_3$ nor simple mixture solution of $IrCl_3$-PVP exhibited any activity (data not shown).The effect of pH and temperature on the activity of PVP-IrNPs was also checked. The result indicated the optimal pH of 4.5, the same as that of native peroxidase (Figure 5C). PVP-IrNPs had relatively broader optimal temperature (35−55 °C) than peroxidase (Figure 5D), which was similar to other nanozymes.[31,55]

Peroxidase-like activity of PVP-IrNPs was evaluated by steady-state kinetics analysis at pH 4.5 and room temperature. Catalytic parameters were obtained by fitting the data to Michiaelis-Menten equation (Figure 6A and B) and Lineweaver−Burk equation (Figure 6C and D). As shown in Table 1, the K_M value of PVP-IrNPs (0.02 mM) was lower than ferritin−platinum NPs (0.22 mM),[28] Co_3O_4 NPs (0.103 mM),[47] Fe_3O_4 NPs (0.098 mM) and natural peroxidase (0.434 mM),[20] suggesting apparently higher affinity of PVP-IrNPs to TMB. Such high affinity might be attributed to the hydrophobic domain of PVP, which displayed similar role as cyclodextrins with hydrophobic cavity in the reported esterase mimic.[56] On the other hand, the K_M value of PVP-IrNPs for H_2O_2 was higher than that of the other enzyme mimic listed in Table 1, indicating that higher H_2O_2 concentration was required to reach maximal reaction rate.

The catalytic efficiency k_{cat} (s^{-1}) was also calculated and compared with other nanoparticles-based enzyme mimics in Table 1. The catalytic efficiency was also normalized by particle surface area.[47] As shown in Table 1, the obtained k_{cat}/area value of PVP-IrNPs for H_2O_2 is much higher than Co_3O_4 and Fe_3O_4 NPs, though lower than platinum-based mimic, Ft-PtNPs (identical to catalase activity mentioned above). However, the peroxidase-like catalytic efficiency of PVP-IrNPs for TMB was highest among Ft-PtNPs, Co_3O_4 and Fe_3O_4. Therefore, PVP-IrNPs indeed are promising peroxidase mimic.

3.4. Mechanism of Peroxidase-like Activity of PVP-IrNPs. According to previous studies, the catalytic pathways of peroxidase-like activity could be generally classified into the electron transfer process, assigned to natural enzyme[57] and Co_3O_4 nanoparticles,[55] and the generation of hydroxyl radical, assigned to iron oxide[46,58] and gold nanoparticles.[27,59] To clarify the catalytic mechanisms of PVP-IrNPs, Rhodamine B oxidation experiment was first performed to check the production of·OH radical. As shown in Figure 7A, the absorbance of Rhodamine B at 550 nm did not change upon incubation with H_2O_2 and increased concentrations of PVP-

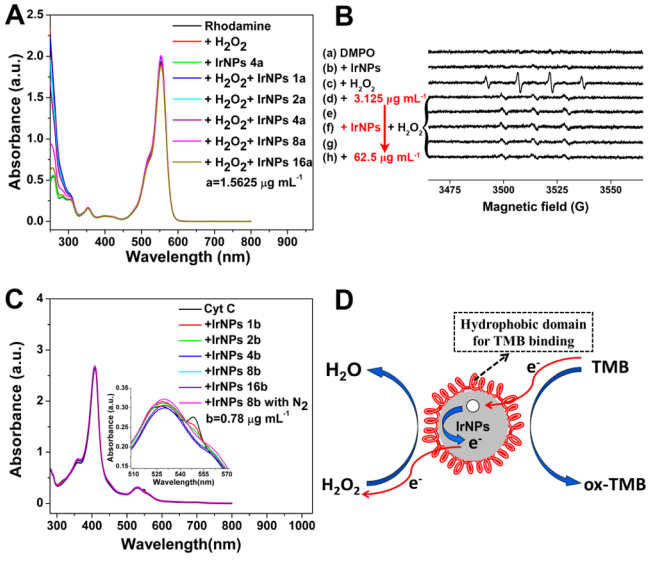

Figure 7. Mechanism of peroxidase-like activities of PVP-IrNPs. (A) Interaction of rhodamine B with PVP-IrNPs, (B) ESR signals of DMPO/•OH spin adduct when incubation of varied concentrations of PVP-IrNPs with H_2O_2 in the presence of DMPO. (C) Electron transfer experiment between cytochrome C (Cyt C) and PVP-IrNPs. (D) Proposed mechanism for the peroxidase-like activity of PVP-IrNPs.

DOI: 10.1021/acsami.5b01271
ACS Appl. Mater. Interfaces 2015, 7, 8233−8242

IrNPs for 3.5 h, excluding the generation of·OH radical during the catalysis.

ESR has been recognized as a direct method to characterize the radical process during enzyme catalysis process.[58,60] Figure 7B shows the ESR spectrum of samples containing DMPO, PVP-IrNPs or H_2O_2 in HCl-KCl buffer (pH = 1.2). No obvious ESR signal attributed to DMPO/$^{\bullet}$OH spin adduct was observed in the presence of PVP-IrNPs only. With increasing concentration of PVP-IrNPs from 3.125 to 62.5 μg mL^{-1}, no DMPO/$^{\bullet}$OH spin adduct was also observed in the presence of H_2O_2. Instead, a new three-line ESR spectrum with relative intensities of 1:1:1 was obtained, representative of the degradation product of DMPO,[61] which was quite different from above results obtained in the PVP-IrNPs/H_2O_2/UV system and previously reported PVP-AuNPs.[59] The exact mechanism of this phenomenon is not clear and needs further study. Nevertheless, based on the knowledge that highly reactive hydroxyl radical may lead to oxidative damage to lipids, proteins and DNA, absence of $^{\bullet}$OH during decomposition of H_2O_2 suggested a great potential of PVP-IrNPs involved in the antioxidant therapeutics.

To verify the PVP-IrNPs mediated electron transfer process from TMB to H_2O_2, cytochrome C (Cyt C) was used to test the accepting electron ability of PVP-IrNPs because Cyt C is an active reactant in the electron transfer process.[47] Interestingly, upon increased concentration of PVP-IrNPs, absorbance at 520 and 550 nm gradually disappeared with the evolution of a new peak at 530 nm (Figure 7C). The corresponding change from reduced state to oxidized state for Cyt C clearly indicated electron transfer from Cyt c to PVP-IrNPs. It should be noted that oxygen was not necessary for the electron transfer process, because similar results were obtained in hypoxia solutions following 0.5 h pumping of pure nitrogen.

All the above results proposed the mechanism of PVP-IrNPs acting as peroxidase (Figure 7D). First, TMB binds to the hydrophobic domains of PVP surrounding the IrNPs, the amino group of which donates lone-pair electrons to IrNPs, leading to increased electron density of PVP-IrNPs. Second, electron-rich PVP-IrNPs transfer electrons to close-by H_2O_2, which further accelerates the electron transfer process between PVP-IrNPs and TMB. Finally, TMB is oxidized into blue derivative and H_2O_2 is reduced to water during this catalytic cycle. This process is similar to the case of graphene oxide, a peroxidase mimic.[24] In a word, PVP-IrNPs act as peroxidase mimic by promoting the electron transfer between TMB and H_2O_2.

3.5. Effect of PVP-IrNPs on H_2O_2-Induced Cellular Oxidative Damage. Hydrogen peroxide is a common reactive oxygen species (ROS) produced in cellular metabolism, such as glucose oxidation catalyzed by glucose oxidase (GOx)[62] and superoxide anion radical scavenging by superoxide dismutase (SOD).[63] In nature, catalase and peroxidase have been evolved to protect cells against H_2O_2-induced oxidative damage.[63] However, in Alzheimer's disease or other pathological cases, cells may reduce or even lose their abilities to decompose H_2O_2, leading to serious DNA and protein structure damage.[64] In our case, small-sized iridium nanoparticles with both catalase and hydrogen peroxidase-like activities can be speculated to protect cells against H_2O_2-induced oxidative damage. A549 human lung cancer cell was used as a cell model.

First, we evaluated the cytotoxicity of PVP-IrNPs against A549 cells by widely used MTT assay. After incubation of different concentrations of iridium nanoparticles for 24 h, the cells treated with up to 250 μg mL^{-1} PVP-IrNPs still kept the viability more than 90% (Figure 8A), indicating good biocompatibility of PVP-IrNPs. Treating A549 with 1 mM H_2O_2 for 45 min resulted in the death of more than half of cells (Figure 8B). However, incubation of cells with varied concentrations of PVP-IrNPs for 20 h before H_2O_2 treatment lead to significantly enhanced cell viability. Figure 8B showed that PVP-IrNPs protected cells against H_2O_2-induced death in a dose-dependent manner. We further used DCFH-DA, a ROS fluorescence probe emitting green fluorescence upon oxidation by ROS, to measure the intracellular ROS level. As indicated in Figure 8C, only weak fluorescence can be seen in the control and PVP-IrNPs treated cells. In contrast, bright green fluorescence signals can be observed in H_2O_2 treated cells, suggesting higher intracellular ROS levels. But cells incubated with PVP-IrNPs before H_2O_2 treatment only displayed much weaker emission. These result demonstrated that PVP-IrNPs

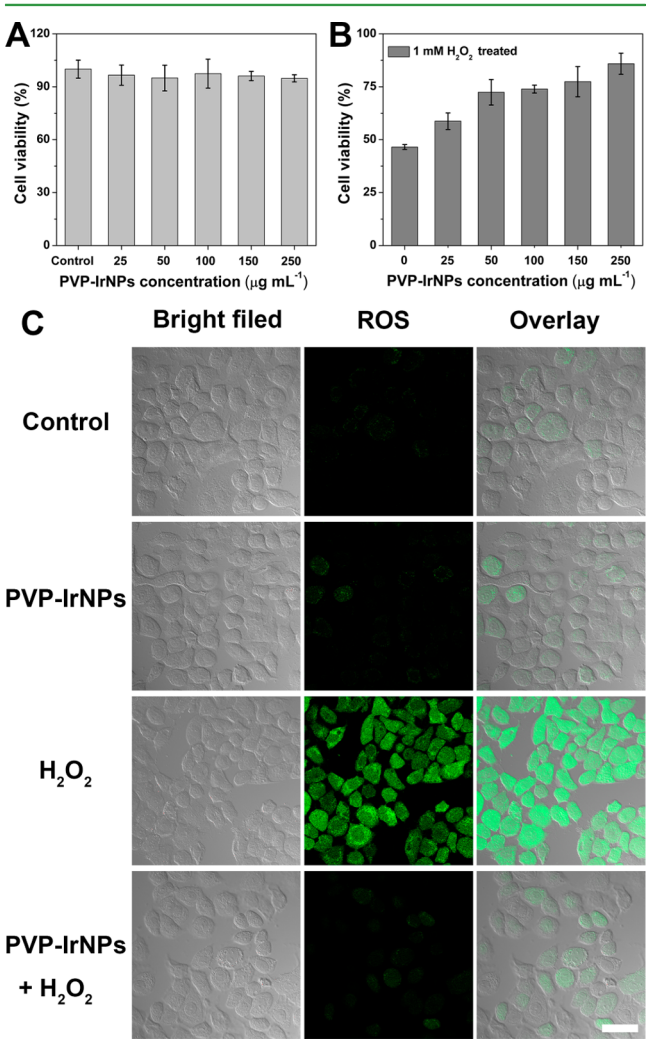

Figure 8. (A) Cytotoxicity of PVP-IrNPs on A549 cells by the MTT assay. (B) The effect of PVP-IrNPs as catalase and peroxidase mimic on H_2O_2-induced cytotoxicity on A549 cells. The data were normalized to control values without PVP-IrNPs and H_2O_2 treatment, which were set as 100% cell viability. (C) The effect of PVP-IrNPs on H_2O_2-induced ROS formation in A549 cells. The cells were incubated with 250 μg mL^{-1} PVP-IrNPs for 20 h and then treated with 1 mM H_2O_2 for 45 min. The intracellular ROS were detected after staining with 50 μM DCFH-DA for 15 min. The scale bars represent 40 μm.

DOI: 10.1021/acsami.5b01271
ACS Appl. Mater. Interfaces 2015, 7, 8233−8242

could be used as a biocompatible antioxidant to reduce H_2O_2-induced cellular oxidative damage.

4. CONCLUSIONS

In summary, PVP-IrNPs were synthesized using a simple green method and the capability acting as catalase and peroxidase mimic was demonstrated. PVP-IrNPs displayed small size (~1.5 nm) and good dispersion. The dual enzyme-like activities of PVP-IrNPs depended on the pH value of reaction medium, showing higher catalase-like activity in neutral and basic pH and higher peroxidase-like activity in slightly acid medium. Kinetics studies found that the catalytic activity of PVP-IrNPs was comparable to reported platinum nanoparticles, and it is worth mentioning that much easier preparation procedures and low cost stabilization agents were utilized. Mechanistic study suggested that the catalase-like activity of PVP-IrNPs was associated with formed oxidized species $Ir(0)@IrO_2$ upon reaction with H_2O_2, while peroxidase-like activity originated from their ability as electron transfer mediators during the catalysis cycle, rather than the generation of hydroxyl radical. Due to their good biocompatibility and antioxidant-like properties, PVP-IrNPs were successfully applied to reduce external H_2O_2-induced intracellular ROS level and protect cells against H_2O_2-induced oxidative damage in an A549 lung cancer cell model. This work will promote the mechanism study and biomedical application of nanomaterials-based enzyme mimics.

■ ASSOCIATED CONTENT

Supporting Information

EDX spectrum of PVP-IrNPs (Figure S1), XPS survey of PVP-IrNPs (Figure S2) and $IrCl_3$-PVP (Figure S3), effects of pH on the oxygen production catalyzed by PVP-IrNPs and catalase during ESR spin label oximetry experiments (Figure S4), TEM images of PVP-IrNPs after reaction with H_2O_2 (Figure S5), XPS characterization of PVP-IrNPs after reaction with H_2O_2 and TMB + H_2O_2 (Figure S6), and reaction scheme of TMB oxidation by peroxidase (Scheme S1). This material is available free of charge via the Internet at http://pubs.acs.org.

■ AUTHOR INFORMATION

Corresponding Author

*E-mail: cesmzw@mail.sysu.edu.cn. Fax: +86-20-8411-2245.

Notes

The authors declare no competing financial interest.

■ ACKNOWLEDGMENTS

This research was supported by the National Natural Science Foundation of China (No. 21231007), 973 Program (No. 2014CB845604), the Ministry of Education of China (Nos. IRT1298 and 313058), Guangdong Provincial Government, and the Fundamental Research Funds for the Central Universities.

■ REFERENCES

(1) Anderson, J. R.; Howe, R. F. Generation of a Supported Iridium Catalyst of Extremely High Dispersion. *Nature* **1977**, *268*, 129−130.

(2) McDaniel, N. D.; Coughlin, F. J.; Tinker, L. L.; Bernhard, S. Cyclometalated Iridium(III) Aquo Complexes: Efficient and Tunable Catalysts for the Homogeneous Oxidation of Water. *J. Am. Chem. Soc.* **2007**, *130*, 210−217.

(3) Hintermair, U.; Sheehan, S. W.; Parent, A. R.; Ess, D. H.; Richens, D. T.; Vaccaro, P. H.; Brudvig, G. W.; Crabtree, R. H. Precursor Transformation During Molecular Oxidation Catalysis with Organometallic Iridium Complexes. *J. Am. Chem. Soc.* **2013**, *135*, 10837−10851.

(4) Shibata, S.; Suenobu, T.; Fukuzumi, S. Direct Synthesis of Hydrogen Peroxide from Hydrogen and Oxygen by Using a Water-Soluble Iridium Complex and Flavin Mononucleotide. *Angew. Chem., Int. Ed.* **2013**, *52*, 12327−12331.

(5) Gao, W.; Pei, A.; Dong, R.; Wang, J. Catalytic Iridium-Based Janus Micromotors Powered by Ultralow Levels of Chemical Fuels. *J. Am. Chem. Soc.* **2014**, *136*, 2276−2279.

(6) He, L.; Tan, C.-P.; Ye, R.-R.; Zhao, Y.-Z.; Liu, Y.-H.; Zhao, Q.; Ji, L.-N.; Mao, Z.-W. Theranostic Iridium(III) Complexes as One- and Two-Photon Phosphorescent Trackers to Monitor Autophagic Lysosomes. *Angew. Chem., Int. Ed.* **2014**, *53*, 12137−12141.

(7) Ma, X.; Jia, J.; Cao, R.; Wang, X.; Fei, H. Histidine−Iridium(III) Coordination-Based Peptide Luminogenic Cyclization and Cyclo-Rgd Peptides for Cancer-Cell Targeting. *J. Am. Chem. Soc.* **2014**, *136*, 17734−17737.

(8) DeRosa, M. C.; Hodgson, D. J.; Enright, G. D.; Dawson, B.; Evans, C. E. B.; Crutchley, R. J. Iridium Luminophore Complexes for Unimolecular Oxygen Sensors. *J. Am. Chem. Soc.* **2004**, *126*, 7619−7626.

(9) Li, G.; Chen, Y.; Wang, J.; Lin, Q.; Zhao, J.; Ji, L.; Chao, H. A Dinuclear Iridium(III) Complex as a Visual Specific Phosphorescent Probe for Endogenous Sulphite and Bisulphite in Living Cells. *Chem. Sci.* **2013**, *4*, 4426−4433.

(10) Rehmann, N.; Ulbricht, C.; Köhnen, A.; Zacharias, P.; Gather, M. C.; Hertel, D.; Holder, E.; Meerholz, K.; Schubert, U. S. Advanced Device Architecture for Highly Efficient Organic Light-Emitting Diodes with an Orange-Emitting Crosslinkable Iridium(III) Complex. *Adv. Mater.* **2008**, *20*, 129−133.

(11) Mani, G.; Feldman, M. D.; Patel, D.; Agrawal, C. M. Coronary Stents: A Materials Perspective. *Biomaterials* **2007**, *28*, 1689−1710.

(12) Crabtree, R. H. Introduction and History. In *Topics in Organometallic Chemistry:Iridium Catalysis*; Andersson, P. G., Ed.; Springer Verlag: Berlin, 2011; pp 1−10.

(13) Källström, K.; Hedberg, C.; Brandt, P.; Bayer, A.; Andersson, P. G. Rationally Designed Ligands for Asymmetric Iridium-Catalyzed Hydrogenation of Olefins. *J. Am. Chem. Soc.* **2004**, *126*, 14308−14309.

(14) Kundu, S.; Liang, H. Shape-Selective Formation and Characterization of Catalytically Active Iridium Nanoparticles. *J. Colloid Interface Sci.* **2011**, *354*, 597−606.

(15) Antolini, E. Iridium as Catalyst and Cocatalyst for Oxygen Evolution/Reduction in Acidic Polymer Electrolyte Membrane Electrolyzers and Fuel Cells. *ACS Catal.* **2014**, *4*, 1426−1440.

(16) Özkar, S.; Finke, R. G. Iridium(0) Nanocluster, Acid-Assisted Catalysis of Neat Acetone Hydrogenation at Room Temperature: Exceptional Activity, Catalyst Lifetime, and Selectivity at Complete Conversion. *J. Am. Chem. Soc.* **2005**, *127*, 4800−4808.

(17) Kobayashi, H.; Yamauchi, M.; Kitagawa, H. Finding Hydrogen-Storage Capability in Iridium Induced by the Nanosize Effect. *J. Am. Chem. Soc.* **2012**, *134*, 6893−6895.

(18) Wei, H.; Wang, E. Nanomaterials with Enzyme-Like Characteristics (Nanozymes): Next-Generation Artificial Enzymes. *Chem. Soc. Rev.* **2013**, *42*, 6060−6093.

(19) Lin, Y.; Ren, J.; Qu, X. Catalytically Active Nanomaterials: A Promising Candidate for Artificial Enzymes. *Acc. Chem. Res.* **2014**, *47*, 1097−1105.

(20) Gao, L.; Zhuang, J.; Nie, L.; Zhang, J.; Zhang, Y.; Gu, N.; Wang, T.; Feng, J.; Yang, D.; Perrett, S.; Yan, X. Intrinsic Peroxidase-Like Activity of Ferromagnetic Nanoparticles. *Nat. Nanotechnol.* **2007**, *2*, 577−583.

(21) Asati, A.; Santra, S.; Kaittanis, C.; Nath, S.; Perez, J. M. Oxidase-Like Activity of Polymer-Coated Cerium Oxide Nanoparticles. *Angew. Chem., Int. Ed.* **2009**, *48*, 2308−2312.

(22) Deng, H.; Shen, W.; Peng, Y.; Chen, X.; Yi, G.; Gao, Z. Nanoparticulate Peroxidase/Catalase Mimetic and Its Application. *Chem.—Eur. J.* **2012**, *18*, 8906−8911.

DOI: 10.1021/acsami.5b01271
ACS Appl. Mater. Interfaces 2015, 7, 8233−8242

(23) Dai, Z.; Liu, S.; Bao, J.; Ju, H. Nanostructured Fes as a Mimic Peroxidase for Biocatalysis and Biosensing. *Chem.—Eur. J.* **2009**, *15*, 4321−4326.
(24) Song, Y.; Qu, K.; Zhao, C.; Ren, J.; Qu, X. Graphene Oxide: Intrinsic Peroxidase Catalytic Activity and Its Application to Glucose Detection. *Adv. Mater.* **2010**, *22*, 2206−2210.
(25) Shi, W. B.; Wang, Q. L.; Long, Y. J.; Cheng, Z. L.; Chen, S. H.; Zheng, H. Z.; Huang, Y. M. Carbon Nanodots as Peroxidase Mimetics and Their Applications to Glucose Detection. *Chem. Commun.* **2011**, *47*, 6695−6697.
(26) Zheng, X.; Liu, Q.; Jing, C.; Li, Y.; Li, D.; Luo, W.; Wen, Y.; He, Y.; Huang, Q.; Long, Y.-T.; Fan, C. Catalytic Gold Nanoparticles for Nanoplasmonic Detection of DNA Hybridization. *Angew. Chem., Int. Ed.* **2011**, *50*, 11994−11998.
(27) Jv, Y.; Li, B.; Cao, R. Positively-Charged Gold Nanoparticles as Peroxidiase Mimic and Their Application in Hydrogen Peroxide and Glucose Detection. *Chem. Commun.* **2010**, *46*, 8017−8019.
(28) Fan, J.; Yin, J.-J.; Ning, B.; Wu, X.; Hu, Y.; Ferrari, M.; Anderson, G. J.; Wei, J.; Zhao, Y.; Nie, G. Direct Evidence for Catalase and Peroxidase Activities of Ferritin-Platinum Nanoparticles. *Biomaterials* **2011**, *32*, 1611−1618.
(29) He, W.; Wu, X.; Liu, J.; Hu, X.; Zhang, K.; Hou, S.; Zhou, W.; Xie, S. Design of AgM Bimetallic Alloy Nanostructures (M = Au, Pd, Pt) with Tunable Morphology and Peroxidase-Like Activity. *Chem. Mater.* **2010**, *22*, 2988−2994.
(30) Tao, Y.; Lin, Y.; Huang, Z.; Ren, J.; Qu, X. Incorporating Graphene Oxide and Gold Nanoclusters: A Synergistic Catalyst with Surprisingly High Peroxidase-Like Activity over a Broad Ph Range and Its Application for Cancer Cell Detection. *Adv. Mater.* **2013**, *25*, 2594−2599.
(31) Zhang, J.-W.; Zhang, H.-T.; Du, Z.-Y.; Wang, X.; Yu, S.-H.; Jiang, H.-L. Water-Stable Metal-Organic Frameworks with Intrinsic Peroxidase-Like Catalytic Activity as a Colorimetric Biosensing Platform. *Chem. Commun.* **2014**, *50*, 1092−1094.
(32) Sharma, T. K.; Ramanathan, R.; Weerathunge, P.; Mohammadtaheri, M.; Daima, H. K.; Shukla, R.; Bansal, V. Aptamer-Mediated 'Turn-Off/Turn-On' Nanozyme Activity of Gold Nanoparticles for Kanamycin Detection. *Chem. Commun.* **2014**, *50*, 15856−15859.
(33) Jiang, H.; Chen, Z.; Cao, H.; Huang, Y. Peroxidase-Like Activity of Chitosan Stabilized Silver Nanoparticles for Visual and Colorimetric Detection of Glucose. *Analyst* **2012**, *137*, 5560−5564.
(34) Zhang, L.; Laug, L.; Münchgesang, W.; Pippel, E.; Gösele, U.; Brandsch, M.; Knez, M. Reducing Stress on Cells with Apoferritin-Encapsulated Platinum Nanoparticles. *Nano Lett.* **2009**, *10*, 219−223.
(35) Long, R.; Mao, K.; Ye, X.; Yan, W.; Huang, Y.; Wang, J.; Fu, Y.; Wang, X.; Wu, X.; Xie, Y.; Xiong, Y. Surface Facet of Palladium Nanocrystals: A Key Parameter to the Activation of Molecular Oxygen for Organic Catalysis and Cancer Treatment. *J. Am. Chem. Soc.* **2013**, *135*, 3200−3207.
(36) Zheng, C.; Zheng, A.; Liu, B.; Zhang, X.-L.; He, Y.; Li, J.; Yang, H.; Chen, G. One-Pot Synthesized DNA-Templated Ag/Pt Bimetallic Nanoclusters as Peroxidase Mimics for Colorimetric Detection of Thrombin. *Chem. Commun.* **2014**, *50*, 13103−13106.
(37) Ge, S.; Liu, F.; Liu, W.; Yan, M.; Song, X.; Yu, J. Colorimetric Assay of K-562 Cells Based on Folic Acid-Conjugated Porous Bimetallic Pd@Au Nanoparticles for Point-of-Care Testing. *Chem. Commun.* **2014**, *50*, 475−477.
(38) Wang, X.; Zhang, Y.; Li, T.; Tian, W.; Zhang, Q.; Cheng, Y. Generation 9 Polyamidoamine Dendrimer Encapsulated Platinum Nanoparticle Mimics Catalase Size, Shape, and Catalytic Activity. *Langmuir* **2013**, *29*, 5262−5270.
(39) Yu, C.-J.; Chen, T.-H.; Jiang, J.-Y.; Tseng, W.-L. Lysozyme-Directed Synthesis of Platinum Nanoclusters as a Mimic Oxidase. *Nanoscale* **2014**, *6*, 9618−9624.
(40) Hirai, H.; Nakao, Y.; Toshima, N. Preparation of Colloidal Transition Metals in Polymers by Reduction with Alcohols or Ethers. *J. Macromol. Sci., Chem.* **1979**, *A13*, 727−750.
(41) McKee, D. W. Catalytic Decomposition of Hydrogen Peroxide by Metals and Alloys of the Platinum Group. *J. Catal.* **1969**, *14*, 355−364.
(42) Li, J.; Jiang, F.; Yang, B.; Song, X.-R.; Liu, Y.; Yang, H.-H.; Cao, D.-R.; Shi, W.-R.; Chen, G.-N. Topological Insulator Bismuth Selenide as a Theranostic Platform for Simultaneous Cancer Imaging and Therapy. *Sci. Rep.* **2013**, *3*, 1−7.
(43) Sun, Y.; Xia, Y. Shape-Controlled Synthesis of Gold and Silver Nanoparticles. *Science* **2002**, *298*, 2176−2179.
(44) Tsunoyama, H.; Sakurai, H.; Negishi, Y.; Tsukuda, T. Size-Specific Catalytic Activity of Polymer-Stabilized Gold Nanoclusters for Aerobic Alcohol Oxidation in Water. *J. Am. Chem. Soc.* **2005**, *127*, 9374−9375.
(45) Chatterjee, S.; Prajapati, R.; Bhattacharya, A.; Mukherjee, T. K. Microscopic Evidence of "Necklace and Bead"-Like Morphology of Polymer-Surfactant Complexes: A Comparative Study on Poly(Vinylpyrrolidone)-Sodium Dodecyl Sulfate and Poly(Diallyldimethylammonium Chloride)-Sodium Dodecyl Sulfate Systems. *Langmuir* **2014**, *30*, 9859−9865.
(46) Chen, Z.; Yin, J.-J.; Zhou, Y.-T.; Zhang, Y.; Song, L.; Song, M.; Hu, S.; Gu, N. Dual Enzyme-Like Activities of Iron Oxide Nanoparticles and Their Implication for Diminishing Cytotoxicity. *ACS Nano* **2012**, *6*, 4001−4012.
(47) Dong, J.; Song, L.; Yin, J.-J.; He, W.; Wu, Y.; Gu, N.; Zhang, Y. Co_3O_4 Nanoparticles with Multi-Enzyme Activities and Their Application in Immunohistochemical Assay. *ACS Appl. Mater. Interfaces* **2014**, *6*, 1959−1970.
(48) Xia, X.; Figueroa-Cosme, L.; Tao, J.; Peng, H.-C.; Niu, G.; Zhu, Y.; Xia, Y. Facile Synthesis of Iridium Nanocrystals with Well-Controlled Facets Using Seed-Mediated Growth. *J. Am. Chem. Soc.* **2014**, *136*, 10878−10881.
(49) Tsai, H.-M.; Yang, S.-J.; Ma, C.-C. M.; Xie, X. Preparation and Electrochemical Activities of Iridium-Decorated Graphene as the Electrode for All-Vanadium Redox Flow Batteries. *Electrochim. Acta* **2012**, *77*, 232−236.
(50) Smith, R. D. L.; Sporinova, B.; Fagan, R. D.; Trudel, S.; Berlinguette, C. P. Facile Photochemical Preparation of Amorphous Iridium Oxide Films for Water Oxidation Catalysis. *Chem. Mater.* **2014**, *26*, 1654−1659.
(51) Collins, G.; Schmidt, M.; McGlacken, G. P.; O'Dwyer, C.; Holmes, J. D. Stability, Oxidation, and Shape Evolution of PVP-Capped Pd Nanocrystals. *J. Phys. Chem. C* **2014**, *118*, 6522−6530.
(52) Lai, C. S.; Hopwood, L. E.; Hyde, J. S.; Lukiewicz, S. ESR Studies of O_2 Uptake by Chinese Hamster Ovary Cells During the Cell Cycle. *Proc. Natl. Acad. Sci. U.S.A.* **1982**, *79*, 1166−1170.
(53) Jacinto, M. J.; Silva, F. P.; Kiyohara, P. K.; Landers, R.; Rossi, L. M. Catalyst Recovery and Recycling Facilitated by Magnetic Separation: Iridium and Other Metal Nanoparticles. *ChemCatChem.* **2012**, *4*, 698−703.
(54) Bianchi, G.; Mazza, F.; Mussini, T. Catalytic Decomposition of Acid Hydrogen Peroxide Solutions on Platinum, Iridium, Palladium and Gold Surfaces. *Electrochim. Acta* **1962**, *7*, 457−473.
(55) Mu, J.; Wang, Y.; Zhao, M.; Zhang, L. Intrinsic Peroxidase-Like Activity and Catalase-Like Activity of Co_3O_4 Nanoparticles. *Chem. Commun.* **2012**, *48*, 2540−2542.
(56) Zhao, M.; Zhang, L.; Chen, H.-Y.; Wang, H.-L.; Ji, L.-N.; Mao, Z.-W. Effect of Hydrophobic Interaction Cooperating with Double Lewis Acid Activation in a Zinc(II) Phosphodiesterase Mimic. *Chem. Commun.* **2010**, *46*, 6497−6499.
(57) Rodríguez-López, J. N.; Lowe, D. J.; Hernández-Ruiz, J.; Hiner, A. N. P.; García-Cánovas, F.; Thorneley, R. N. F. Mechanism of Reaction of Hydrogen Peroxide with Horseradish Peroxidase: Identification of Intermediates in the Catalytic Cycle. *J. Am. Chem. Soc.* **2001**, *123*, 11838−11847.
(58) Voinov, M. A.; Pagán, J. O. S.; Morrison, E.; Smirnova, T. I.; Smirnov, A. I. Surface-Mediated Production of Hydroxyl Radicals as a Mechanism of Iron Oxide Nanoparticle Biotoxicity. *J. Am. Chem. Soc.* **2010**, *133*, 35−41.

DOI: 10.1021/acsami.5b01271
ACS Appl. Mater. Interfaces 2015, 7, 8233−8242

(59) He, W.; Zhou, Y.-T.; Wamer, W. G.; Hu, X.; Wu, X.; Zheng, Z.; Boudreau, M. D.; Yin, J.-J. Intrinsic Catalytic Activity of Au Nanoparticles with Respect to Hydrogen Peroxide Decomposition and Superoxide Scavenging. *Biomaterials* **2013**, *34*, 765−773.
(60) Liu, Y.; Wu, H.; Li, M.; Yin, J.; Nie, Z. Ph Dependent Catalytic Activities of Platinum Nanoparticles with Respect to the Decomposition of Hydrogen Peroxide and Scavenging of Superoxide and Singlet Oxygen. *Nanoscale* **2014**, *6*, 11904−11910.
(61) Bosnjakovic, A.; Schlick, S. Spin Trapping by 5,5-Dimethylpyrroline-N-Oxide in Fenton Media in the Presence of Nafion Perfluorinated Membranes: Limitations and Potential. *J. Phys. Chem. B* **2006**, *110*, 10720−10728.
(62) Huggett, A. S. G.; Nixon, D. A. Use of Glucose Oxidase, Peroxidase and O-Dianisidine in Determination of Blood and Urinary Glucose. *Lancet* **1957**, *270*, 368−370.
(63) Giorgio, M.; Trinei, M.; Migliaccio, E.; Pelicci, P. G. Hydrogen Peroxide: A Metabolic By-Product or a Common Mediator of Ageing Signals? *Nat. Rev. Mol. Cell Biol.* **2007**, *8*, 722−728.
(64) Roberts, R. A.; Smith, R. A.; Safe, S.; Szabo, C.; Tjalkens, R. B.; Robertson, F. M. Toxicological and Pathophysiological Roles of Reactive Oxygen and Nitrogen Species. *Toxicology* **2010**, *276*, 85−94.

DOI: 10.1021/acsami.5b01271
ACS Appl. Mater. Interfaces 2015, 7, 8233−8242